Stress Intensity Factor solutions for through-clad and underclad defects in WWER reactor pressure vessel nozzles under pressurised thermal shock

Vitalii Antonchenko
LLC "IPP-Centre", Kyiv 01013, Ukraine
Ternopil Ivan Puluj National Technical University, 56, Ruska Str., Ternopil, 46001, Ukraine
antonchenko-vo@ipp-centre.com.ua, https://orcid.org/0000-0003-2210-5308

Yaroslav Dubyk
LLC "IPP-Centre", Kyiv 01013, Ukraine
Karpenko Physico-Mechanical Institute of the NAS of Ukraine, Lviv 79060, Ukraine
dubyk-yr@ipp-centre.com.ua, https://orcid.org/0000-0002-4327-412X

Volodymyr Iasnii
Ternopil Ivan Puluj National Technical University, 56, Ruska Str., Ternopil, 46001, Ukraine
v_iasnii@tntu.edu.ua, https://orcid.org/0000-0002-5768-5288

ABSTRACT. This study develops stress intensity factor (SIF) solutions for cladded WWER reactor pressure vessel nozzles subjected to pressurised thermal shock loading. Although finite element analysis is widely used for fracture assessment, analytical or semi-analytical SIF formulations remain important for fast evaluation, including online stress monitoring, probabilistic fracture mechanics, and screening of transient scenarios. The proposed approach combines an influence coefficient method based on three-dimensional finite-element J-integral evaluation with least-squares refinement of shape coefficients. A stress decomposition procedure is applied to address the stress discontinuity at the ferritic base metal–austenitic cladding interface. The resulting coefficients are validated against finite element reference solutions for representative pressure and thermal loading cases and show good agreement over the investigated range of crack sizes and aspect ratios. The

Citation: Antonchenko, V., Dubyk, Y., Iasnii, V., Stress intensity factors for through clad and underclad defects in a WWER type reactor pressure vessel in pressurised thermal shock analysis, Fracture and Structural Integrity, 77 (2026) 247-264.

Received: 09.04.2026
Accepted: 28.04.2026
Published: 05.05.2026
Issue: 07.2026

developed solutions provide a practical tool for engineering assessment of through-clad and underclad defects in cladded WWER nozzle regions.

KEYWORDS. PTS analysis, Polynomial solution, Stress intensity factor, Fracture of the cladded component.

INTRODUCTION

Brittle fracture assessment is a central requirement in the safety justification of nuclear first-class equipment, and the reactor pressure vessel (RPV) holds particular importance in this context. The allowable operating time of an RPV is ultimately governed by its resistance to brittle fracture, whose margin degrades with neutron irradiation over the plant lifetime. The overall assessment procedure is separated into two complementary tasks: characterisation of the material fracture toughness and its evolution under ageing, and evaluation of the stress intensity factor (SIF) driving any postulated defect. The present work addresses the second task and, more specifically, the development of analytical or semi-analytical SIF solutions suited for rapid engineering evaluation in WWER-1000 nozzle regions containing austenitic cladding.

Although three-dimensional finite element analysis (FEA) is now standard practice for fracture mechanics calculations in the nuclear industry, there remains a strong practical need for fast, closed-form or tabulated SIF solutions. Such solutions are indispensable in probabilistic fracture mechanics (PFM), where Monte Carlo sampling across large populations of postulated flaws requires enormous numbers of individual SIF evaluations. As noted by the FAVOR code developers and subsequent users [1], the ability to evaluate SIFs through weight-function or influence-coefficient look-up rather than repeated finite element runs is essential for computationally tractable PFM assessments. Fast solutions are equally valuable for online stress monitoring, conservative screening of transient scenarios, and inclusion in national regulatory standards.

The structural integrity of RPVs during pressurised thermal shock (PTS) events has been the subject of extensive international research and codification. PTS loading, arising from the injection of cold emergency coolant into a hot and pressurised primary circuit, produces steep thermal gradients that, when combined with repressurisation, can generate large tensile stresses at the inner wall of the vessel. The IAEA has published dedicated guidelines for PTS analysis of WWER-type reactors [2], which prescribe both deterministic and—where uncertainty levels are high—probabilistic approaches to integrity assessment. The IAEA TECDOC- [3] demonstrated that, despite the overall similarity of the PTS problem for PWR and WWER designs, significant differences exist among codes and methodologies, particularly in the treatment of defect characterisation and SIF computation, underlining the need for reactor-type-specific solutions. For WWER-type plants, the VERLIFE unified procedure [4] provides validated guidelines for resistance against fast fracture, covering both deterministic fracture mechanics and, in its more recent revisions, probabilistic approaches for RPV and primary piping lifetime assessment. A comprehensive framework specifically adapted to WWER conditions has also been reported in the open literature [5].

Nozzle regions are recognised as critical locations for RPV integrity, because the geometric discontinuity at the nozzle-to-shell junction produces stress concentrations that can exceed those in the beltline shell even when the neutron fluence is lower. This is reflected in U.S. regulatory requirements that extend pressure–temperature (P–T) limit calculations beyond the beltline to include nozzle materials [6]. The primary regulatory sources for SIF calculation in nozzle geometries are the API 579-1/ASME FFS-1 standard [7] and ASME Boiler and Pressure Vessel Code, Section XI [8]. These documents provide analytical and semi-empirical solutions for circular or quarter-elliptical corner cracks in nozzle regions and are widely referenced in the literature for P–T limit evaluation [4,6,9]. However, a fundamental limitation of the ASME formulations is that they were derived for geometrically uniform, uncladded components and do not account for the bi-material interface between the ferritic base metal and the austenitic cladding layer that is characteristic of actual WWER pressure vessels.

The mechanical response of RPV nozzle corner cracks under combined pressure and thermal loading has been investigated by a number of authors using three-dimensional FEA. Lee and Chou [10] evaluated SIFs for nozzle corner cracks in PWR and BWR geometries under both internal pressure and thermal transients, demonstrating that the ASME circular-crack formula is conservative for that crack shape but can underestimate SIFs for elliptical geometries. Dedicated adjusted magnification factor formulas were proposed to correct for the non-circular case. Chapuliot [11] studied SIF solutions for both sharp and bevelled nozzle corners, providing analytical tools specifically aimed at fatigue crack growth evaluation under cyclic thermal loading. Wang et al. [12] recently extended the influence coefficient method (ICM) to the nozzle corner crack problem, developing SIF solutions valid for arbitrary stress distributions applied to the crack face; their formulation was validated against FEA reference solutions over a range of crack sizes. Lu et al. [13] conducted a comprehensive parametric

numerical study of nozzle corner crack SIFs in RPVs, yielding tabulated solutions that facilitate rapid engineering assessment. The engineering critical assessment framework for nozzle corner cracks under PTS transients—including the effect of cladding on crack initiation—was systematically examined by Li et al. [9], who applied a failure assessment diagram approach to evaluate critical crack sizes under multiple transient scenarios.

The ICM—also referred to in the literature as the influence function method—is a well-established superposition framework in which the SIF under an arbitrary stress distribution is expressed as a linear combination of polynomial stress coefficients multiplied by pre-computed shape (influence) coefficients. The mathematical foundation traces to the weight function theory of Buckner and Rice, and practical influence coefficient databases for cylindrical pressure vessel geometries were developed early on by Keeney and Bryson [14] for clad cylinders, providing tabulated coefficients for semi-elliptical inner-surface flaws over a range of aspect ratios and cladding thicknesses. The FAVOR code, widely used for PFM assessment of U.S. RPVs, relies on weight-function based SIF evaluation for surface-breaking flaws including cladding effects [1].

A distinctive feature of cladded RPVs is the stress discontinuity that arises at the ferritic base metal–austenitic cladding interface due to the mismatch in thermal expansion coefficient and elastic modulus between the two materials. Under PTS conditions, this mismatch produces a localised stress concentration in the cladding and modifies the stress distribution seen by sub-surface cracks. Early finite element studies noted that the presence of cladding generally reduces the SIF under internal pressure loading by suppressing crack opening at the inner wall, but can increase the SIF under thermal loading by superimposing additional tensile stresses in the base metal [15].

For defects that straddle the cladding–base metal interface—the through-clad and underclad crack configurations addressed in the present study—the most directly relevant prior work is that of Marie and Chapuliot [16]. These authors proposed an improved procedure for calculating SIFs of underclad and through-clad defects in RPV cylindrical shell sections subjected to PTS loading, using a polynomial decomposition of the stress field and pre-computed shape factors to handle the stress discontinuity at the interface. The approach separates the total stress field into a component acting through the full ferritic wall thickness and a supplementary component localised within the cladding, allowing the two contributions to the SIF to be evaluated independently and then combined.

Notwithstanding the body of work summarised above, a gap remains for SIF solutions that simultaneously (i) address the three-dimensional nozzle geometry of WWER-1000 vessels with cladding, (ii) cover both through-clad and underclad defect types, (iii) employ the ICM with an explicit interface stress decomposition, and (iv) provide coefficients in a tabular form suitable for direct inclusion in national standards. Existing solutions are either limited to cylindrical shell sections without the nozzle geometry [14, 16], restricted to uncladded geometries [9-12], or do not provide the decomposed cladding coefficients needed to treat the bi-material interface rigorously. The present paper addresses this gap by developing SIF solutions based on three-dimensional FE J-integral evaluation combined with a least-squares refinement of polynomial shape coefficients, validated against FE reference solutions for representative PTS loading cases. Our primary goal is to develop a simple, fast tool for SIF assessment of WWER reactor pressure vessels. The ultimate objective is to produce practical tabulated coefficients specific to WWER-1000 nozzle geometry for integration into Ukrainian national standards.

This paper uses several methodologies for determining shape coefficients. The first step is the influence coefficient method. The second is the refinement of the coefficients using the least-squares method. Both the first and second methods are based on FE model results obtained with a crack inserted into the mesh. The last idea implemented in the paper is to come up with a simple equation for through-clad and under-clad defects for express SIF evaluation.

THE INFLUENCE COEFFICIENT METHOD

FE model and methodology

Fig. 1 shows meshes for a crack with a depth of 10% of the total wall thickness of the RPV, with ellipse semi-axis ratios a/c of 0.3 and 0.7.

In our work, we consider the nozzle part of the reactor vessel with the following parameters: inner radius Ri = 1991 mm, ferrite part thickness h = 345 mm, and cladding thickness r = 9 mm. The nozzle forging itself has a complex geometry, with shell thickening, and the thickness to be used in analysis is ambiguous. In this case, the value h = 345 mm is the smallest distance from the crack centre to the external surface.

Fig. 1 shows a model with a crack depth of 10% of the total thickness of the RPV wall and an ellipse semi-axis ratio a/c = 0.3. Considering the symmetry conditions, a finite element model (FEM) representing half of the crack was created. We used three-dimensional solid elements to build the model. The mesh has 205,148 elements and 216,901 nodes. The average orthogonal quality is 0.8922. The element size near the crack tip can vary widely, depending on the crack's geometric dimensions. If we use a constant element size around the crack front, the largest crack will have the largest mesh size. In all

the considered FE models, the size of the finite element around the crack front is as follows: the radius of the first contour is 0.01 mm, and the radius of the outermost contour is 0.14 mm. The element dimension along the crack front is 2 mm.

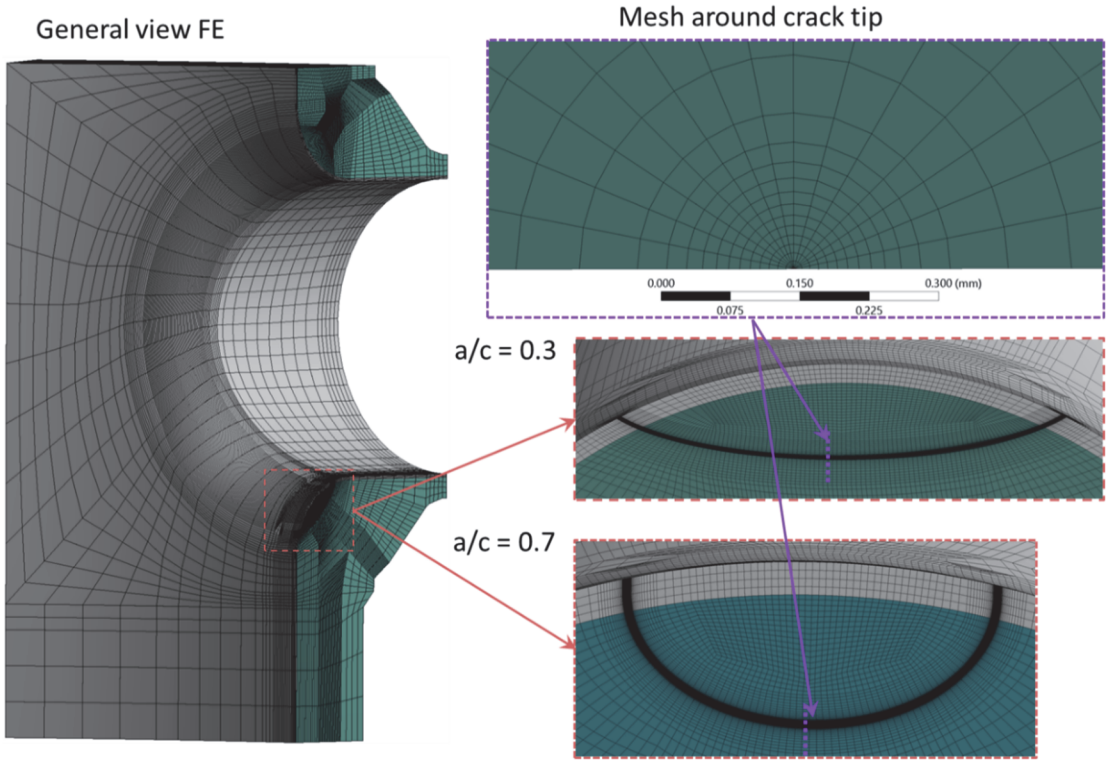

Figure 1: Model of reactor vessel nozzle with built-in crack.

The Tab. 1 shows the values of elasticity modules for BM and cladding. The data is taken from VERLIFE [4].

Temperature, °C	20	100	200	300	350
Cladding	165	160	153	146	142
Base metal	208	201	193	183	177.5

Table 1: Modulus of elasticity, GPa.

To calculate the SIF, we will use ICM: From the FEM results we obtain the value of the J-integral along the crack tip. We assume that the plane deformation conditions are satisfied along the full crack tip. Therefore, the stress intensity coefficient KI was obtained using the J-integral. The following expression is used to obtain the shape factor for each degree of the polynomial:

$$i_j = \frac{\sqrt{E^* J}}{\left(\frac{a+r}{b+r}\right)^j \sqrt{\pi(a+r)}} \tag{1}$$

where the parameter E^*:

$$E^* = \frac{E}{1-\mu} \tag{2}$$

When using quadratic elements, the average value of the shape factor for each element should be calculated. For the deepest point of the crack, the three nodes of the element are used: point 1, point 2 and point 3 as represented in Fig. 2.

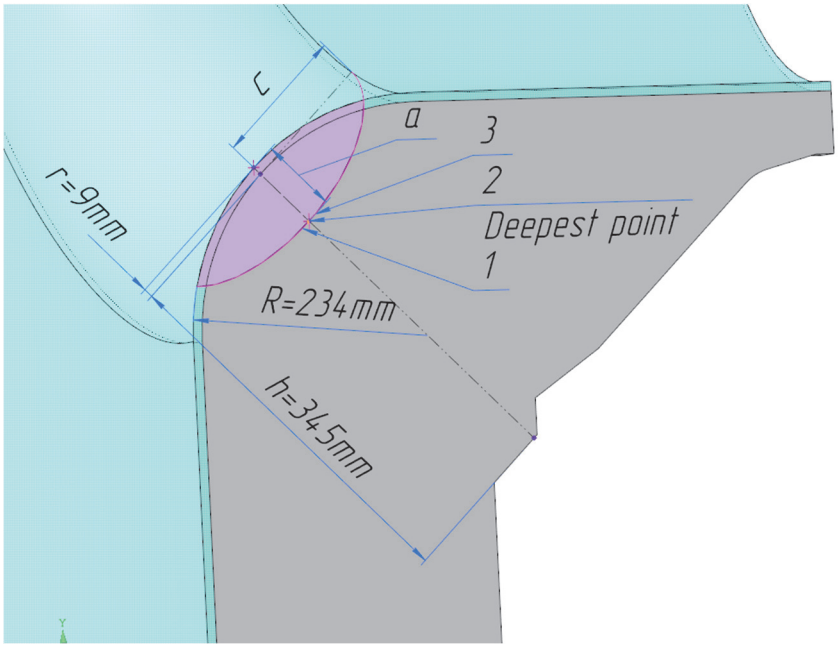

Figure 2: Parameters of the considered defect, with point representation.

The average shape functions are obtained from the following relations:

$$i = \frac{1}{6}\left(i_{point\,1} + 4 \cdot i_{point\,2} + i_{point\,3}\right) \tag{3}$$

The WWER-1000 reactor pressure vessel has anticorrosion cladding, which significantly complicates the accurate determination of stress polynomials. Due to the abrupt change in material properties within the cladding region, substantial errors arise when approximating the stress field.

Fig. 3 presents the distributions of the actual stresses obtained from the finite element analysis as well as their interpolated representations. The analysis of the stress plots clearly demonstrates the pronounced influence of the anticorrosion cladding on the stress distribution. The solid blue line corresponds to the actual stresses, while the red dashed line represents the interpolated function.

During the interpolation process, a significant error is observed near the cladding, due to the inability of a smooth polynomial function to capture the steep stress gradients adequately. This error may lead to either overestimation or underestimation of the stress level near the crack tip, thereby affecting the accuracy of subsequent fracture mechanics parameter calculations.

In Fig. 3, we can see a stress discontinuity in the cladding zone, making accurate polynomial selection impossible with this distortion. Therefore, we applied the stress decomposition method presented in VERLIFE [4]. It consists of separating the stresses in the base metal and the cladding. We obtain two smooth functions. The stress decomposition process is schematically shown in Fig. 4.

Then SIF can be found using equation:

$$K_1 = \left(\sum_{j=0}^{4} \sigma_j i_j \left(\frac{a+r}{h+r}\right)^j + \sum_{j=0}^{1} \sigma_{jr} i_{jr} \left(\frac{a+r}{h+r}\right)^j\right)\sqrt{\pi\left(a+r\right)} \tag{4}$$

Stress intensity factor analysis is based on the linear elastic fracture mechanics, thus we decompose the complex stress distribution to compute the SIF separately for each type of polynomial loading. The most convenient way is to apply different polynomial loading on the crack surface.

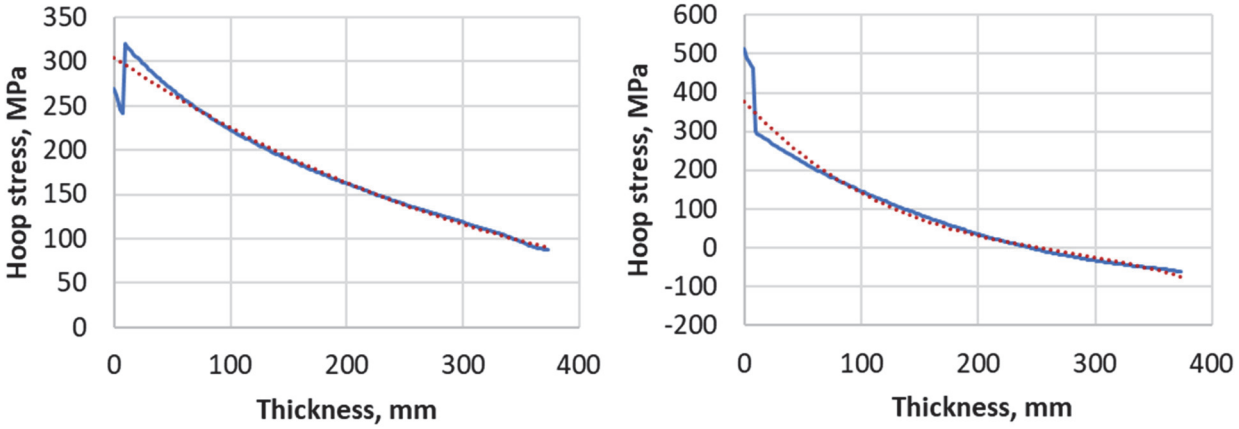

Figure 3: Options for interpolating operating stresses, left – heat-up, right cool-down.

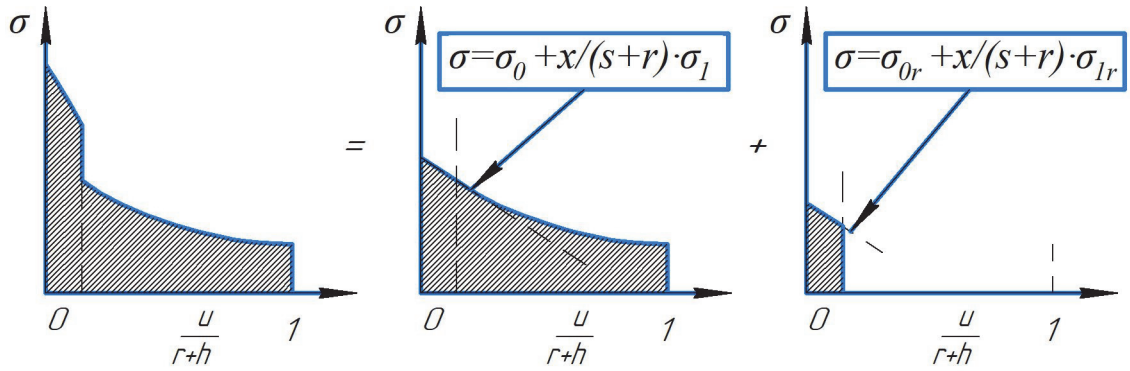

Figure 4: Separation of stresses.

Boundary conditions

ICM works with the results of the FE model calculation. Therefore, it is necessary to calculate the stress distribution and the SIF (J integral) value. The same model is used to calculate SIF (J integral) and stress distribution, only the boundary conditions in the crack zone change, e.g. crack surface is either loaded, or symmetry condition is applied.

The following boundary conditions were used to calculate the FEM:

- Symmetry condition. The plane of symmetry passes through the crack edge. For the SIF (J integral) calculation, the crack surface is not included in the boundary condition. For the stress field calculation, the crack surface is included in the boundary condition.
- Restriction of vertical displacement on the model's bottom part.
- Frictionless boundary conditions on the other vertical end of the model.
- Load on the crack surface, in case of SIF (J integral) calculations.
- "End-cap" axial force for the nozzle.

The load on the crack surface is used to determine the stress polynomials. The load on other surfaces is used to determine the stress distribution and the SIF (J integral). The specified boundary conditions are shown in Fig. 5.

The ICM method applies an external load directly to the crack faces, i.e. to determine the SIF arising from a predefined load, by varying the form and surface of load application, the shape coefficients are determined. Those different forms of loading are used to describe the effect of the applied load in the coefficients of polynomials from zero to fourth order. The shape coefficients are calculated separately for the base metal and the cladding, which reflects the material heterogeneity and differences in mechanical properties of two layers.

Coefficients determined by the ICM

After performing FEM calculations with the applied load at the crack tip, we obtained the J integral value, Jint. Using expression (1), we find the values of the shape coefficients.

Tab. 2 – Tab. 5 show the shape coefficients for surface and subsurface cracks in the RPV nozzle. We considered a wide range of crack sizes from 5% to 15% and ellipse axis ratios of 0.3 and 0.7.

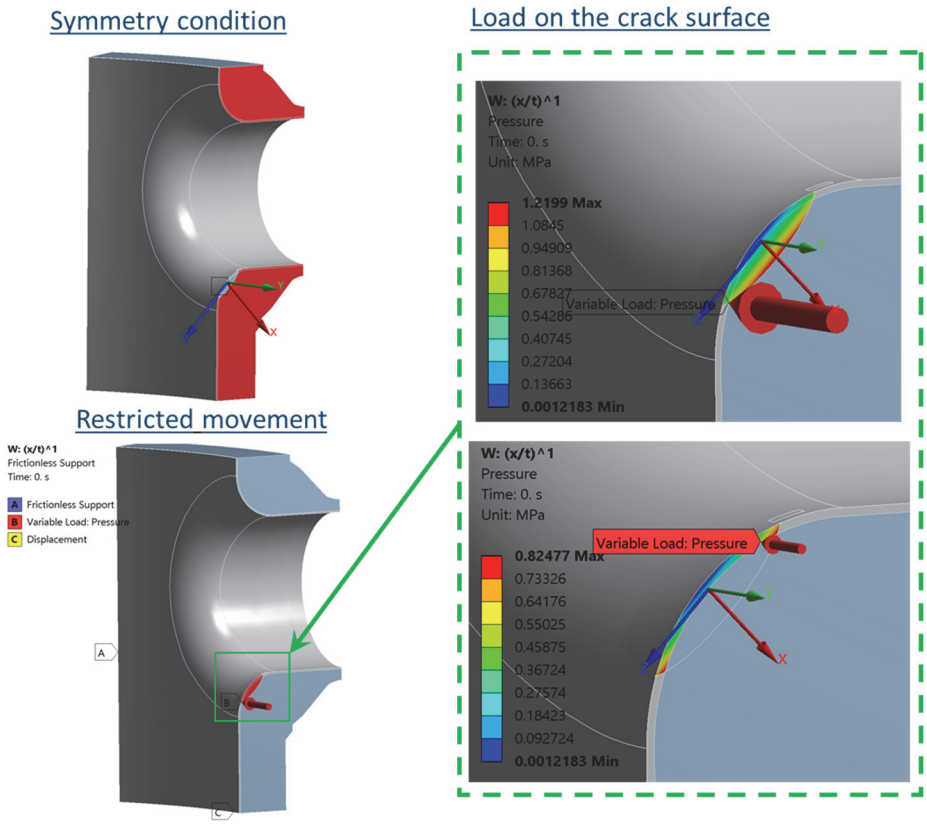

Figure 5: Boundary conditions for polynomial calculations of SIF values

	Size, %	i_0	i_1	i_2	i_3	i_{r0}	i_{r1}
$E_1/E_2 = 1$	5	0.9136	0.5538	0.4067	0.3225	0.2094	0.0414
	7.5	0.9165	0.5593	0.4108	0.3257	0.1611	0.0283
	10	0.9145	0.5686	0.4226	0.3388	0.1283	0.0216
	12.5	0.9113	0.5630	0.4146	0.3291	0.1094	0.0179
	15	0.9104	0.5658	0.4177	0.3321	0.0950	0.0156
$E_1/E_2 = 0.7$	5	0.9445	0.5660	0.4137	0.3276	0.2247	0.0439
	7.5	0.9399	0.5676	0.4149	0.3282	0.1706	0.0296
	10	0.9328	0.5705	0.4259	0.3407	0.1345	0.0223
	12.5	0.9265	0.5684	0.4173	0.3307	0.1139	0.0183
	15	0.9235	0.5708	0.4204	0.3338	0.0983	0.0160

Table 2: Shape factors for TCC with axis ratios of 0.3.

	Size, %	i_0	i_1	i_2	i_3	i_{r0}	i_{r1}
$E_1/E_2 = 1$	5	0.6720	0.4435	0.3419	0.2795	0.1083	0.0189
	7.5	0.7028	0.4578	0.3506	0.2857	0.0900	0.0125
	10	0.7176	0.4652	0.3552	0.2891	0.0759	0.0092
	12.5	0.7264	0.4695	0.3576	0.2907	0.0661	0.0074
	15	0.7343	0.4739	0.3604	0.2927	0.0589	0.0064
$E_1/E_2 = 0.7$	5	0.6954	0.4515	0.3458	0.2817	0.1204	0.0209
	7.5	0.7210	0.4639	0.3535	0.2874	0.0977	0.0136
	10	0.7325	0.4702	0.3575	0.2904	0.0813	0.0098
	12.5	0.7403	0.4744	0.3600	0.2920	0.0701	0.0078
	15	0.7450	0.4776	0.3621	0.2937	0.0618	0.0066

Table 3: Shape factors for TCC with axis ratios of 0.7

	Size, %	i_0	i_1	i_2	i_3
$E_1/E_2 = 1$	5	0.6823	0.5329	0.4321	0.3600
	7.5	0.6903	0.5244	0.4187	0.3456
	10	0.6996	0.5238	0.4158	3.3154
	12.5	0.7010	0.5180	0.4083	0.3351
	15	0.7060	0.5181	0.4076	0.3343
$E_1/E_2 = 0.7$	5	0.6987	0.5426	0.4381	0.3640
	7.5	0.7066	0.5333	0.4239	0.3490
	10	0.7157	0.5322	0.4206	0.3457
	12.5	0.7165	0.5257	0.4127	0.3378
	15	0.7213	0.5258	0.4121	0.3372

Table 4: Shape factors for UCC with axis ratios of 0.3.

	Size, %	i_0	i_1	i_2	i_3
$E_1/E_2 = 1$	5	0.6054	0.4779	0.3910	0.3282
	7.5	0.6150	0.4731	0.3819	0.3183
	10	0.6213	0.4702	0.3767	0.3128
	12.5	0.6256	0.4678	0.3728	0.3087
	15	0.6301	0.4672	0.3710	0.3068
$E_1/E_2 = 0.7$	5	0.6161	0.4839	0.3946	0.3305
	7.5	0.6256	0.4786	0.3850	0.3202
	10	0.6319	0.4753	0.3795	0.3145
	12.5	0.6370	0.4733	0.3757	0.3105
	15	0.6402	0.4718	0.3734	0.3082

Table 5: Shape factors for UCC with axis ratios of 0.7.

Validation of the obtained coefficients

To validate the obtained coefficients, several practically important cases were studied: internal pressure, temperature gradient, the combined effect of the above factors.

Fig. 6 shows the stress distribution graph for the combined pressure and temperature load case. The left figure shows the stress for the case E_{clad}/E_{BM} =1, and the right figure shows the case E_{clad}/E_{BM}=0.7. The right figure shows the stress polynomial function for the base metal, with stresses separated into those in the base metal and those in the cladding.

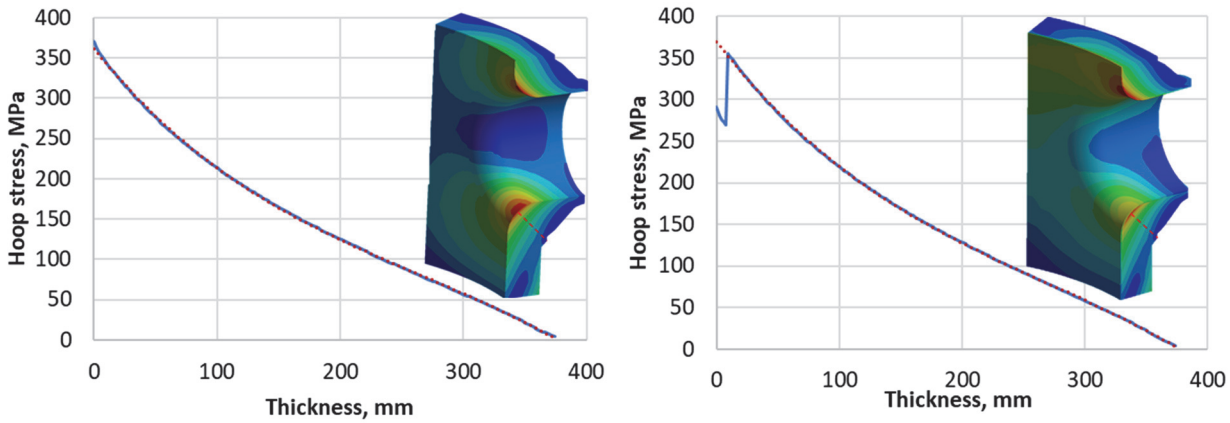

Figure 6: Stress distribution and polynomial for combined loading: left - E_{clad}/E_{BM} =1; right E_{clad}/E_{BM}=0.7.

Tab. 6 presents the results of verification calculations of test cases and existing formulas for evaluating SIF for a through-clad cracks.
Tab. 7 presents the results of verification calculations of test cases for a underclad cracks. The tables present the results for a defect with a depth of 10% and an ellipse axis ratio of 0.3 and 0.7.

	Case	FEM, MPa√m		Current approach, MPa√m		Δ, %		Ref [7] radiusc	Δ, %		Ref [8] sharp	Δ, %		Ref [11] radius	Δ, %		Ref [11] sharp	Δ, %	
		0.3	0.7	0.3	0.7	0.3	0.7	-	0.3	0.7	-	0.3	0.7	-	0.3	0.7	-	0.3	0.7
$E_1/E_2 = 1$	Pressure	63.4	49.4	62.3	48.6	-1.73	-1.60	56.9	-10.1	15.2	58.3	-8.0	18.0	49.4	-22.0	0.0	42.2	-33.3	-14.5
	Quadratic temperature distribution	44.4	34.4	43.6	34.0	-1.62	-1.32	39.9	-10.1	15.8	40.8	-8.0	18.6	35.4	-20.2	2.9	26.1	-41.3	-24.3
	All the power factors	107.6	83.7	105.8	82.6	-1.64	-1.37	96.8	-10.0	15.6	99.1	-7.9	18.4	84.8	-21.2	1.3	68.3	-36.5	-18.4
$E_1/E_2 = 0.7$	Pressure	62.9	49.7	61.9	48.8	-1.56	-1.63	54.4	-13.5	9.5	55.7	-11.4	12.1	46.6	-25.9	-6.2	98.1	56.0	97.5
	Quadratic temperature distribution	45.6	35.7	45.0	35.2	-1.22	-1.19	39.7	-12.8	11.4	40.7	-10.8	14.0	35.0	-23.1	-1.8	51.7	13.4	44.9
	All the power factors	108.3	85.2	106.9	84.1	-1.29	-1.30	94.1	-13.1	10.5	96.3	-11.0	13.1	81.6	-24.7	-4.2	149.7	38.3	75.8

Table 6: Comparison of test cases for a 10% through-clad defect.

	Case	FEM, MPa√m		Current approach, MPa√m		Δ, %	
		0.3	0.7	0.3	0.7	0.3	0.7
$E_1/E_2 = 1$	Pressure	42.1	37.4	39.9	36.7	-5.26	-1.94
	Quadratic temperature distribution	29.0	25.7	27.2	25.3	-6.06	-1.63
	All the power factors	71.0	63.0	71.3	62.1	0.50	-1.38
$E_1/E_2 = 0.7$	Pressure	44.0	38.9	43.3	38.1	-1.72	-1.92
	Quadratic temperature distribution	30.8	27.1	30.3	26.7	-1.55	-1.62
	All the power factors	74.8	65.9	73.6	64.8	-1.52	-1.65

Table 7: Comparison of test cases for a 10% underclad defect.

Fig. 7 shows the normalized SIF values for a through-clad defect. The results are presented for a pressure load case.

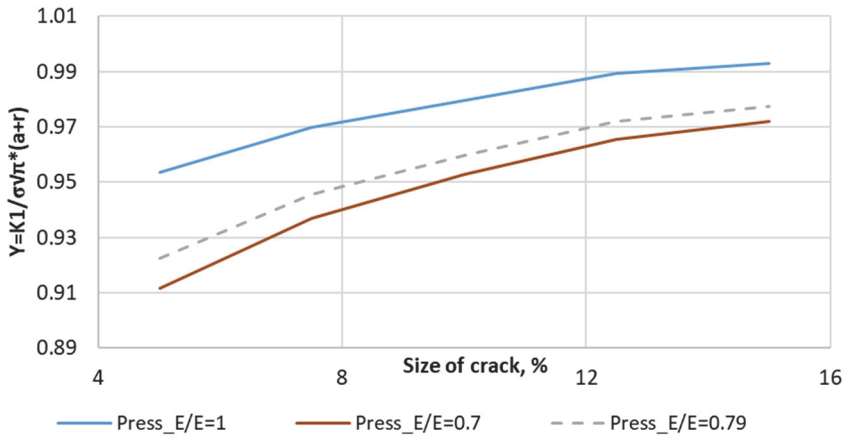

Figure 7: Normalized SIF values for a through-clad defect, for a pressure load case.

From the results presented in Tab. 6 and Tab. 7, we can see that the SIF values calculated using our coefficients are in good agreement with the FEM results, but have a slight error of 2%. Therefore, we tried to improve the accuracy of these coefficients using the least squares method. These coefficients were used as the initial value in the solution.

THE LEAST SQUARE APPROXIMATION

The least squares method (LSM) is a statistical approach used to determine the optimal approximation to the solution of an overdetermined system by minimizing the sum of squared deviations between experimental data and the corresponding theoretical values. In the referenced source [10], a system of equations for determining the stress intensity factor for a surface flaw is presented. Based on expression (5), a system of equations was derived for a nozzle configuration without considering a corrosion-resistant cladding layer.

$$K_1 = \left[A_0 M_0 + A_1 \left(\frac{2a}{\pi} \right) M_1 + A_2 \left(\frac{a^2}{2} \right) M_2 + A_3 \left(\frac{4a^3}{3\pi} \right) M_3 \right] \sqrt{\pi a} \tag{5}$$

Using expression (5) for through-clad defects results in an error of 15-20% in both the lower and upper directions. This is especially true for small crack sizes. Therefore, we suggest accounting for the stress discontinuity at the cladding-to-base metal interface by writing down system 5 with shape coefficients in the cladding.

$$\sqrt{\pi(a+r)} \cdot \begin{bmatrix} A_{10} & A_{11}\left(\frac{2(a+r)}{\pi}\right) & A_{12}\left(\frac{(a+r)^2}{2}\right) & A_{13}\left(\frac{4(a+r)^3}{3\pi}\right) & A_{10r} \\ & \vdots & & & \\ A_{n0} & A_{n1}\left(\frac{2(a+r)}{\pi}\right) & A_{n2}\left(\frac{(a+r)^2}{2}\right) & A_{n3}\left(\frac{4(a+r)^3}{3\pi}\right) & A_{n0r} \end{bmatrix}_{n\times 5} \cdot \begin{bmatrix} M_0 \\ M_1 \\ M_2 \\ M_3 \\ M_{0r} \end{bmatrix}_{5\times 1} = \begin{bmatrix} K_1 \\ \vdots \\ K_n \end{bmatrix}_{n\times 1} \tag{6}$$

Based on expression (4), we write a system of equations to determine the shape coefficients for the ICM method. In this variant, the least-squares method is used to obtain a more accurate solution based on the shape coefficient values presented in Tab. 2 - Tab. 5.

$$\sqrt{\pi(a+r)} \cdot \begin{bmatrix} \sigma_{10}\sigma_{11}\left(\frac{a+r}{h+r}\right) & \sigma_{12}\left(\frac{a+r}{h+r}\right)^2 & \sigma_{13}\left(\frac{a+r}{h+r}\right)^3 & \sigma_{10r}\sigma_{11r}\left(\frac{a+r}{h+r}\right) \\ & \vdots & & \\ \sigma_{n0}\sigma_{n1}\left(\frac{a+r}{h+r}\right) & \sigma_{n2}\left(\frac{a+r}{h+r}\right)^2 & \sigma_{n3}\left(\frac{a+r}{h+r}\right)^3 & \sigma_{n0r}\sigma_{n1r}\left(\frac{a+r}{h+r}\right) \end{bmatrix}_{n\times 6} \cdot \begin{bmatrix} i_0 \\ i_1 \\ i_2 \\ i_3 \\ i_{0r} \\ i_{1r} \end{bmatrix}_{6\times 1} = \begin{bmatrix} K_1 \\ \vdots \\ K_n \end{bmatrix}_{n\times 1} \tag{7}$$

Equation systems (6) and (7) are formulated for a through-clad defects. However, by excluding the cladding thickness r and the corresponding coefficients M_{0r}, i_{0r}, i_{1r}, these equations can be adapted for a subclad defect. Equation systems (6) and (7) differ not only in the coefficients associated with the stress polynomial terms, but also in the form of the polynomials themselves. The polynomial expansion expressions are presented below: Eqn. (8) is used for system (6), whereas Eqn. (9) is applied to system (7).

$$\sigma = A_0 + A_1 x + A_2 x^2 + A_3 x^3 \tag{8}$$

$$\sigma = \sigma_0 + \sigma_1 \frac{x}{h+r} + \sigma_2 \left(\frac{x}{h+r} \right)^2 + \sigma_3 \left(\frac{x}{h+r} \right)^3 \tag{9}$$

Coefficients determined by least squares method

The least-squares method requires a large amount of input data to determine the average solution, so the system of Eqns. (7) must be overdetermined. During the first iteration of this method, 10 boundary states representing the theoretical operating conditions of the reactor vessel were specified. However, during simulations of real accident scenarios, the stress intensity factor values calculated using the obtained coefficients showed significant errors, exceeding 10% in some cases. This indicates that the specified set of boundary conditions does not fully capture the conditions encountered in real accident scenarios. In this regard, an attempt was made to form a system of Eqns. (7) based on two emergency scenarios, followed by verification of the accuracy of calculations for three other scenarios.

The left side of Fig. 8 presents the stress distributions for two accident scenarios. The LOCA scenario is characterized as a transient process with a large temperature gradient across the reactor vessel wall thickness under low internal pressure. The OTHER scenario is characterized as a transient process with combined loading due to pressure and temperature gradient, or a low temperature gradient and high internal pressure. Also, for the solution, it is necessary to have the SIF value for each type and size of crack. The right side of Fig. 8 shows the SIF value for a through-clad defect with a depth of 10% and a half-axis ratio of 0.3.

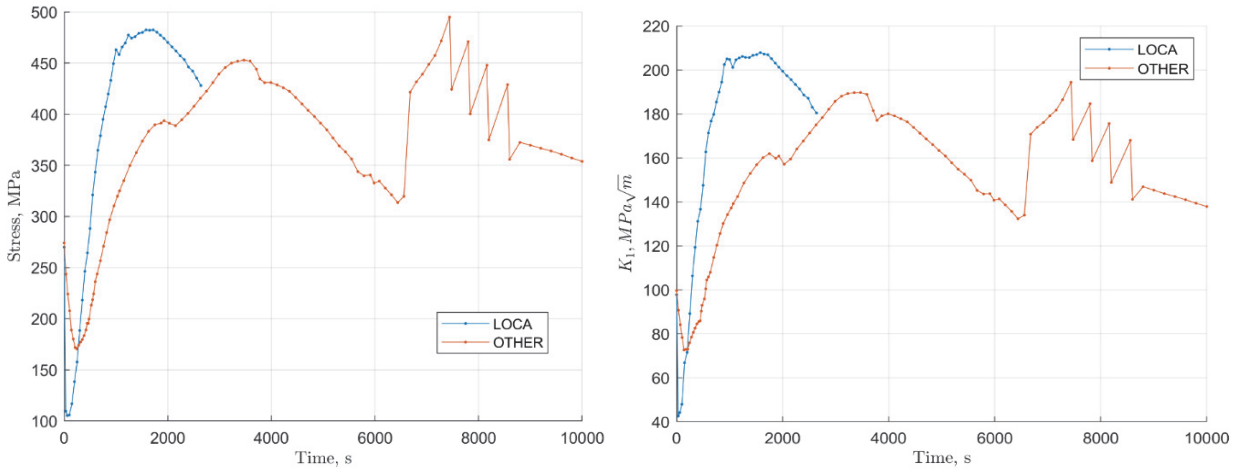

Figure 8: Stress at the defect location and SIF for a through-clad defect depth of 10%.

To determine the coefficients $i_{0..3,\ r0,r1}$, we will write down the system of Eqns. (7) for each type and size of crack. As a first approximation, the results from Tab. 2 – Tab. 5 were used. In the operating temperature range of the RPV, the ratio of the Young's moduli of the cladding and base metal is almost constant and approximately equal to 0.78. Therefore, the interpolated values of the shape coefficients were used for the calculation. This system is overdetermined, so the values of $i_{0..3,\ r0,r1}$ and must satisfy all values of the system.

	Size, %	i_0	i_1	i_2	i_3	i_{r0}	i_{r1}
$E_1/E_2 = 1$	5	0.9512	0.5421	0.3560	0.1964	0.2316	0.0425
	7.5	0.9479	0.5485	0.4216	0.6293	0.1789	0.0258
	10	0.9412	0.5501	0.4244	0.5182	0.1449	0.0164
	12.5	0.9348	0.5568	0.4482	0.5153	0.1194	0.0103
	15	0.9118	0.5132	0.3226	0.1222	0.1057	0.0078
$E_1/E_2 = 0.7$	5	0.7045	0.4408	0.2907	0.2014	0.1259	0.0276
	7.5	0.7317	0.4649	0.3813	0.6321	0.1042	0.0173
	10	0.7440	0.4698	0.3588	0.3803	0.0890	0.0113
	12.5	0.7507	0.4775	0.3681	0.3351	0.0769	0.0073
	15	0.7559	0.4827	0.3759	0.3249	0.0668	0.0049

Table 8: Refined Chapuliot coefficients TCD.

	Size,%	i_0	i_1	i_2	i_3
$E_1/E_2=1$	5	0.7144	0.5577	0.4730	0.8785
	7.5	0.7228	0.5516	0.4932	0.9121
	10	0.7280	0.5418	0.4572	0.5983
	12.5	0.7299	0.5387	0.4560	0.5134
	15	0.7178	0.5005	0.3455	0.1666
$E_1/E_2=0.7$	5	0.6331	0.4981	0.3957	0.6587
	7.5	0.6414	0.4988	0.4529	0.8715
	10	0.6470	0.4873	0.3932	0.4395
	12.5	0.6496	0.4831	0.3816	0.3321
	15	0.6520	0.4818	0.3836	0.3185

Table 9: Refined Chapuliot coefficients UCC.

Fig. 9 and Fig. 10 show the results for other groups of accident scenarios. The graphs show the results of FEM and those based on the refined coefficients determined by system (7). The results for all types of cracks are similar, so only one scenario for one type of crack is presented. It can be seen that the coefficients obtained by the least-squares method are more accurate than those determined by the direct ICM.

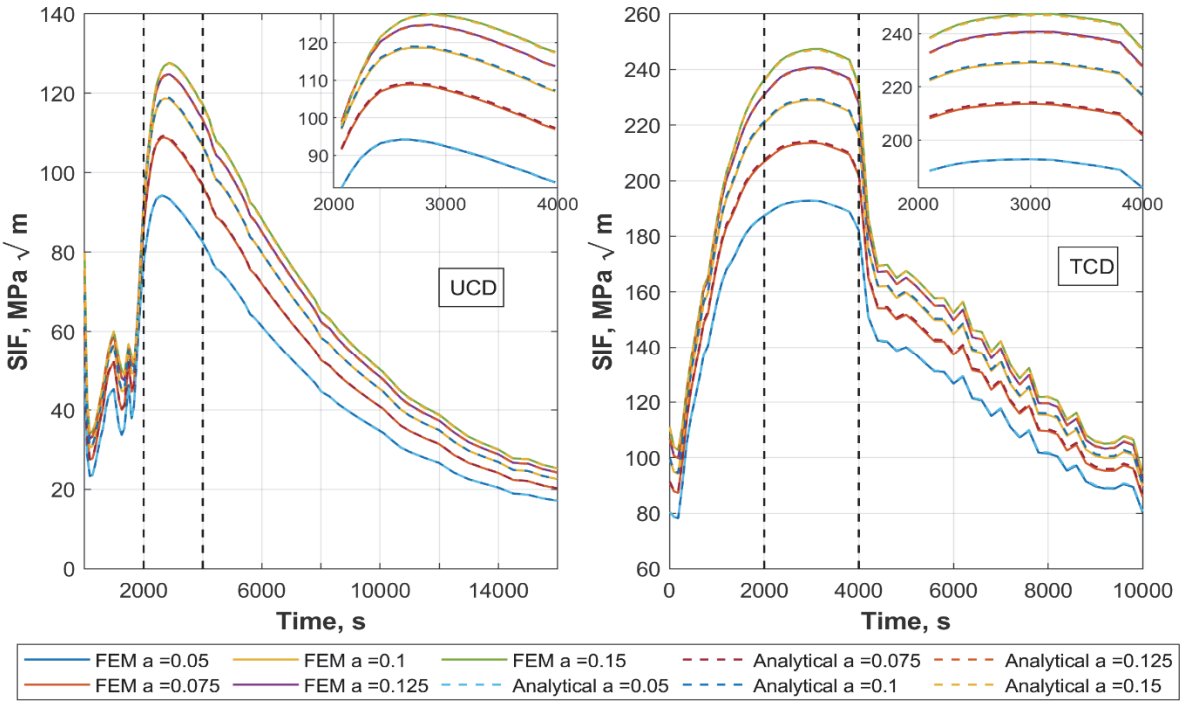

Figure 9: SIF in time for LOCA and MSLB test accident scenarios, a/c=0.3.

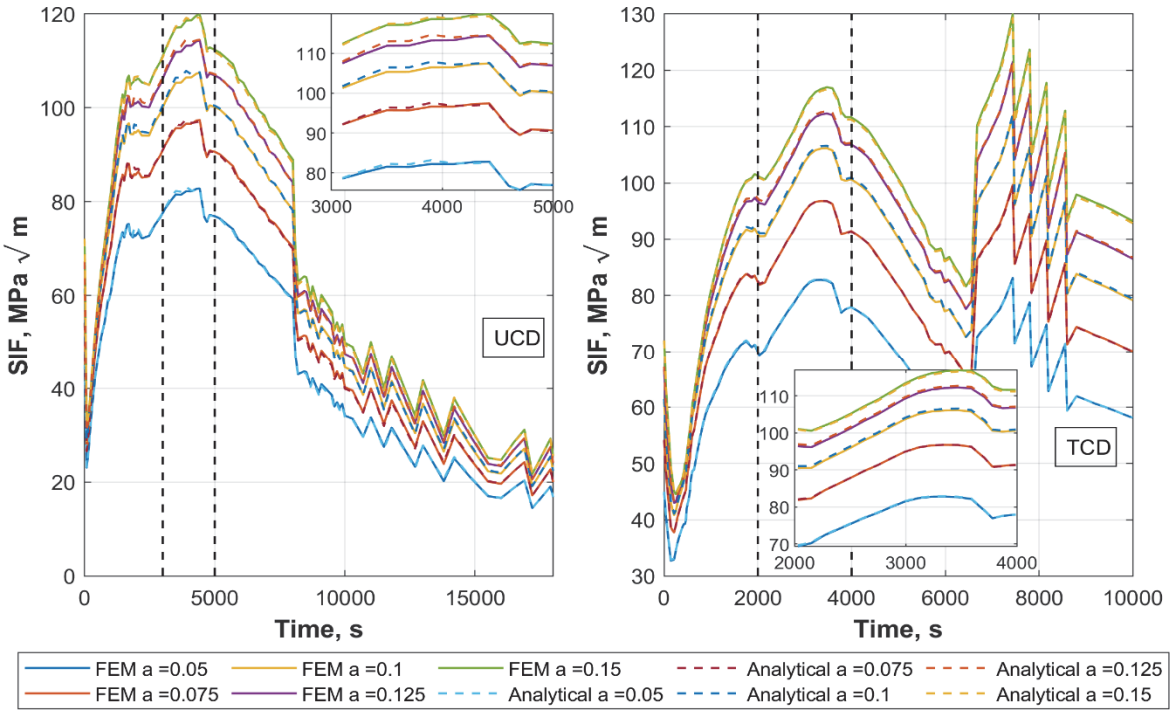

Figure 10: SIF in time for PRISE and OTHER test accident scenarios, a/c=0.7.

GENERALIZED SOLUTION FOR ALL CRACK SIZES

Modification of the ellipticity factor

The ellipticity factor Q is used as a convenient unifying parameter to describe the influence of the semi-elliptical crack tip shape on the stress intensity factor. It is included in the geometry (shape) function and accounts for the effect of the ratio of crack depth to its half-length, a/c, which determines the curvature of the crack tip. As a result, the complex three-dimensional geometry of a semi-elliptical crack tip can be represented by a single dimensionless parameter, thereby significantly simplifying engineering calculations. The use of this coefficient ensures the standardization of analytical approaches while simplifying the evaluation procedure. This is why the ellipticity coefficient has become widely used in engineering methods for crack analysis and has been incorporated into a number of regulatory documents, including the API 579-1/ASME FFS-1 standards [7] and the ASME Code for Boilers and Pressure Vessels, Section XI [8]. The ellipticity factor can be determined from expression (10).

$$Q = 1 + 1.464\left(\frac{a}{c}\right)^{1.65} \tag{10}$$

The ellipticity factor reported in the literature was derived from the complete elliptic integral of the second kind, which effectively corresponds to the dimensionless length of a quarter of the ellipse's arc. This approach is appropriate when the classical semi-elliptical shape approximates the crack tip. However, in the actual nozzle geometry, the crack is located at the radius fillet, and its crack tip does not extend to an angle of $\pi/2$, leading to a deviation from the classical geometric model. Therefore, in this work, it is proposed to use modified ellipticity factors obtained from numerical calculations using the finite element method.

We determine the ratio $SIF_{0.3}/SIF_{0.7}$ based on the FEM results. Fig. 11 shows the dependence of this ratio on the crack size, with each curve corresponding to a separate time step in the accident scenario.

An analysis of results for a non-stationary thermal process reveals variability in defect behavior. A high stability of the SIF ratio characterizes defects located beneath the austenitic cladding. The cladding acts as a thermal and mechanical barrier, smoothing the thermal gradient and ensuring the constancy of boundary conditions. In this case, the effect of ellipticity remains predictable and is almost independent of the crack size or the stage of thermal shock. For cracks that extend directly to the surface of a fillet, there is significant variability in the values of the ratio $SIF_{0.3}/SIF_{0.7}$, which depends on both the

defect size and the calculated step of the accident scenario. This is because, unlike under-cladding defects, where the austenitic cladding mechanically restrains the opening of the crack edges, a surface crack lacks this stabilizing effect. Accordingly, we observe the defect's response to an increase in size, leading to its front covering a larger area of the metal. This means that the defect interacts with a broader range of local boundary conditions, determined by both the fillet curvature and the significant length of the front, through which the surface crack introduces significant irregularities in the temperature field.

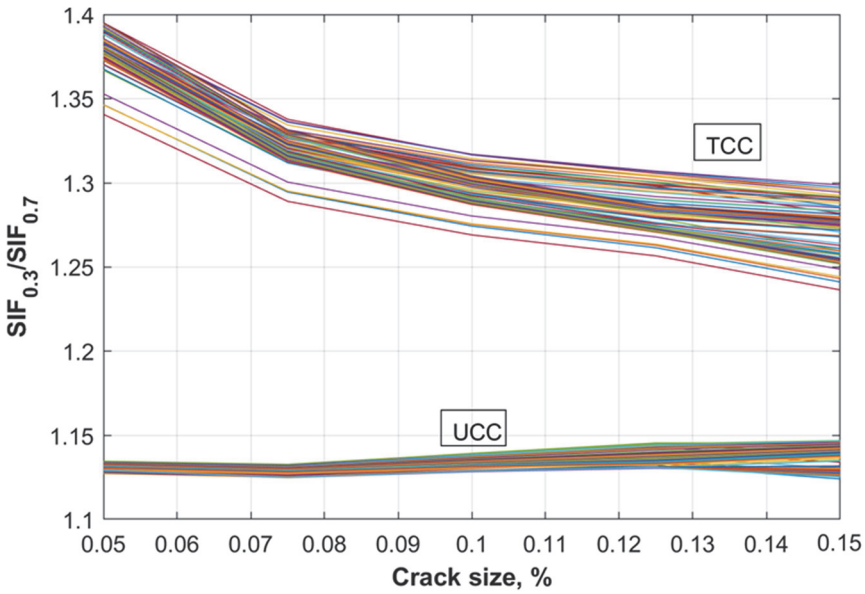

Figure 11: The relationship between $SIF_{0.3}$ and $SIF_{0.7}$ with respect to the relative crack depth.

Let's express the ratio $SIF_{0.3}/SIF_{0.7}$ using the generalized SIF equation with a geometric shape factor for cracks with ellipticity of 0.3 and 0.7.

$$\frac{K_{0,3}}{K_{0,7}} = \frac{\sigma \cdot \sqrt{\frac{\pi a}{Q_{0,3}}}}{\sigma \cdot \sqrt{\frac{\pi a}{Q_{0,7}}}} \tag{11}$$

After simplifying the expression, we find that the ratio does not depend on the crack depth, but depends solely on the ellipticity factor Q.

$$\frac{Q_{0,7}}{Q_{0,3}} = \left(\frac{K_{0,3}}{K_{0,7}}\right)^2 = X \tag{12}$$

Let's write down the expression 10 in terms of the coefficients A and B, and substitute it into Eqn. (12) to get

$$B = \frac{A \cdot (1 - X)}{X \cdot \left(\frac{a}{c_{0.3}}\right)^{1.65} - \left(\frac{a}{c_{0.7}}\right)^{1.65}} \tag{13}$$

Using expression 13, we will find the coefficient B for each crack when A = 1. The surface crack is constructed such that the thickness of the weld deposit increases the depth a but does not increase the major axis c of the ellipse; therefore, this must be taken into account when determining the coefficient B. Based on the calculations, a linear function describing the

variation in the coefficient B was derived, generalizing the solution across five crack sizes. The expressions for determining the shape coefficient will take the following form:

$$Q_{UCC} = 1 + \left(-0.384 \cdot \frac{a}{t} + 0.761 \right) \cdot \left(a / c \right)^{1.65} \tag{14}$$

$$Q_{TCC} = 1 + \left(-2.85 \cdot \frac{a}{t} + 1.766 \right) \cdot \left(a / c \right)^{1.65} \tag{15}$$

Single equation for through-clad and underclad defects

The use of exact solutions is sometimes redundant and only complicates calculations, particularly when determining SIF for intermediate crack sizes. In view of this, a generalized approach was developed based on the system of Eqns. (6), allowing for solutions to be found for defects with depths ranging from 5% to 15% of the wall thickness and for arbitrary crack ellipticity. To improve the results, a modified elliptical coefficient was applied using expressions (14) and (15) for underclad and surface cracks, respectively. The final mathematical dependencies for calculating the SIF are presented in the form of Eqns. (16) and (17).

The data presented in Fig. 8 was used for the calculation. Tab. 10 ppresents the generalized shape coefficients for through-clad defects and underclad defects.

$$K_1 = \left[A_0 M_0 + A_1 \left(\frac{2a}{\pi} \right) M_1 + A_2 \left(\frac{a^2}{2} \right) M_2 + A_3 \left(\frac{4a^3}{3\pi} \right) M_3 \right] \sqrt{\frac{\pi a}{Q_{UCC}}} \tag{16}$$

$$K_1 = \left[A_0 M_0 + A_1 \left(\frac{2a}{\pi} \right) M_1 + A_2 \left(\frac{a^2}{2} \right) M_2 + A_3 \left(\frac{4a^3}{3\pi} \right) M_3 + A_{0r} M_{0r} \right] \sqrt{\frac{\pi a}{Q_{TCC}}} \tag{17}$$

	M_0	M_1	M_2	M_3	M_{r0}
UCC	0.7394	0.9862	0.9616	0.0399	-
TCC	1.0865	1.1753	1.3892	2.1169	0.1042

Table 10: Generalized coefficients.

Fig. 12 and Fig. 13 present the results of the SIF calculations during the accident scenario. The calculations were performed using the generalized shape factor values given in Tab. 10. The graphs presented show that the results obtained using the generalized solution are in good agreement with those from the FEM. For the largest crack, a slight underestimation of the stress intensity factor values is observed, whereas for smaller cracks the calculated SIF values are conservative. Overall, this indicates acceptable accuracy of the proposed generalized approach for analyzing accident scenarios.

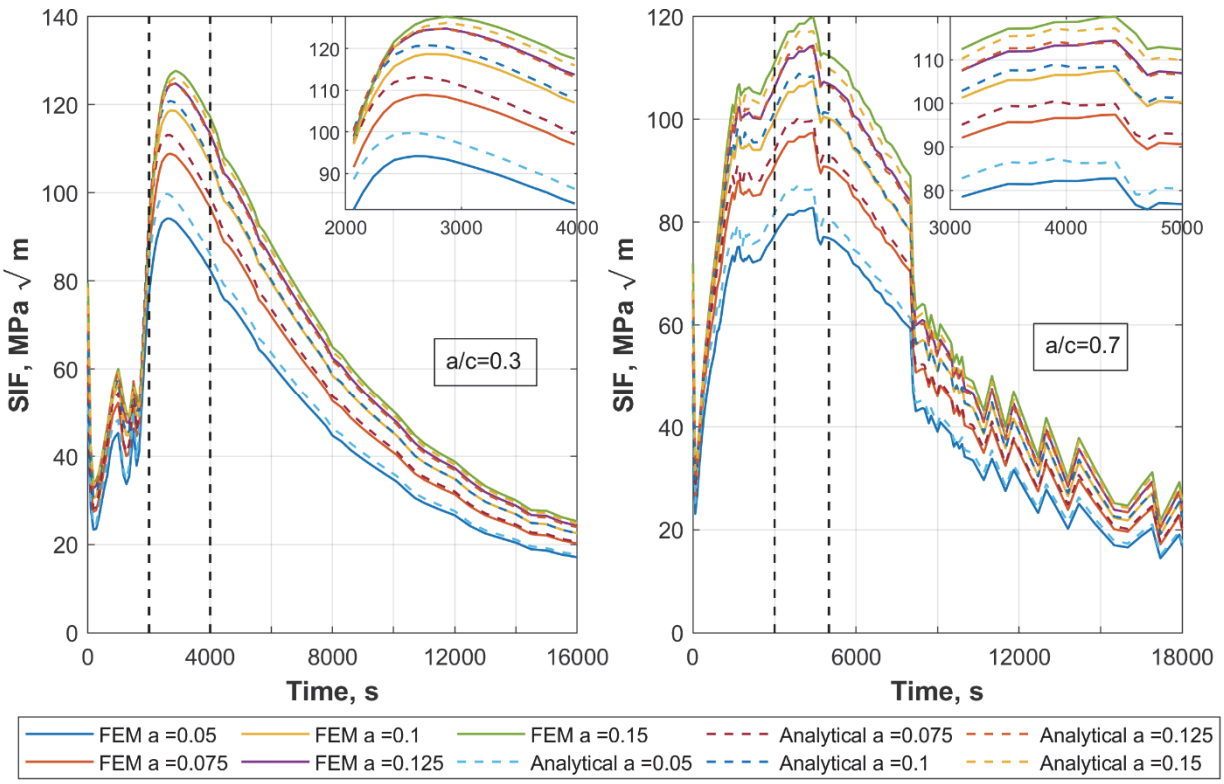

Figure 12: SIF in time for LOCA and PRISE test accident scenarios, UCC.

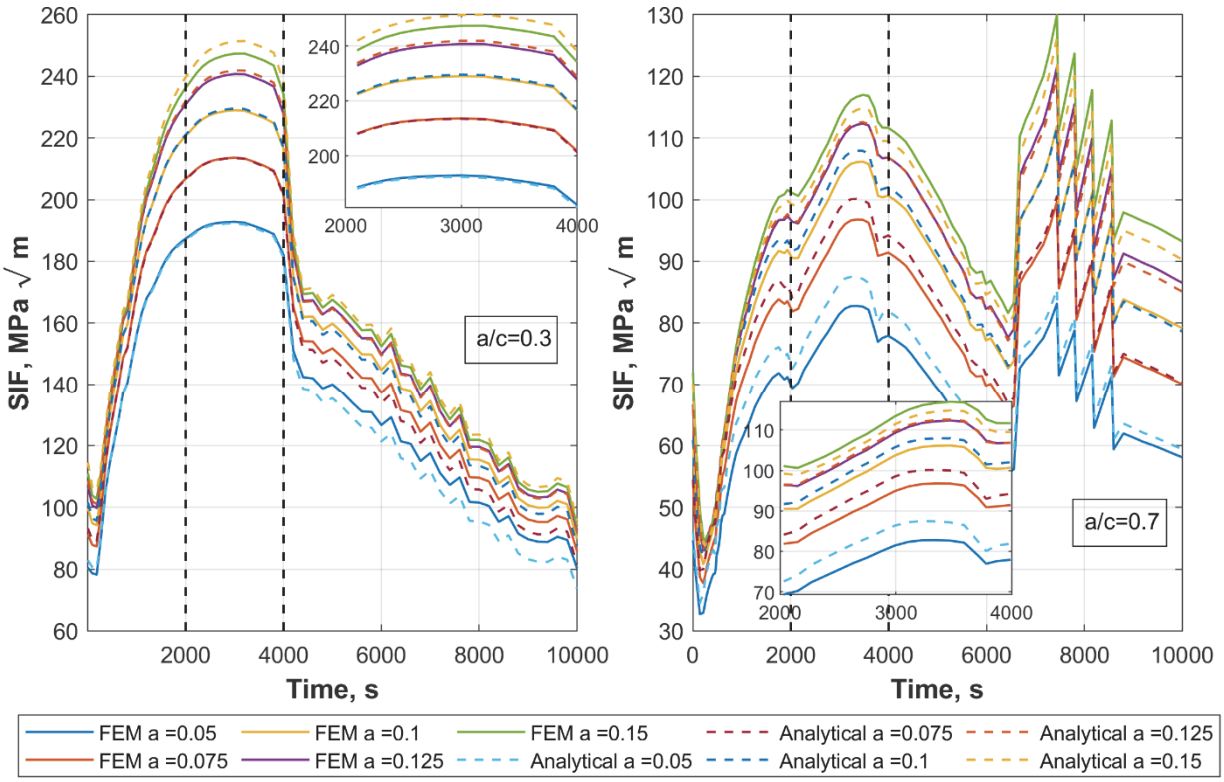

Figure 13: SIF in time for MSLB and OTHER test accident scenarios, a/c=0.7.

CONCLUSIONS

This study assessed analytical methods for evaluating stress intensity factors in cladded WWER reactor pressure-vessel nozzles under pressurized thermal-shock conditions. The following conclusions can be drawn:

- Accurate representation of the stress discontinuity introduced by corrosion-resistant cladding is essential, particularly for shallow surface and through-clad defects; neglecting this effect can lead to SIF deviations on the order of 20% for small cracks.
- The influence coefficient method delivers accurate SIF estimates but requires high-quality finite element meshes and careful numerical implementation near the crack front.
- The least-squares refinement improves robustness and accuracy when calibrated using representative transient scenarios and yields coefficients that reproduce finite-element reference SIF values with deviations of approximately 2% for the verification cases considered.

Overall, the proposed coefficients and the generalized solution offer a practical, computationally efficient tool for engineering fracture assessments of cladded WWER nozzle regions.

NOMENCLATURE

R_i	inner radius of vessel
r	cladding thickness
h	thickness of the ferritic vessel
E,μ	Young's modulus, Poisson ratio
σ	normal to the crack surface stress
i	polynomial coefficients
K_I	stress intensity factor
J	J integral (Jint)
c,a	crack length, crack depth
Q	elliptical coefficient
σ_j, A_j	stress polynomial coefficients
i_j, M_j	shape factors
RPV	Reactor Pressure Vessel
SIF	Stress Intensity Factor
FEM	Finite Element Method / Finite Element Model
PTS	Pressurized thermal shock
ICM	Influence coefficient method
LSM	Least square method
FEM/FEA	Finite element model/analysis

REFERENCES

[1] Spencer B., Hoffman W., Jiang W. (2022). Weight function procedure for reduced order fracture analysis of arbitrary flaws in cylindrical pressure vessels, Int. J. Press. Vessels Pip. DOI: https://doi.org/10.1016/j.ijpvp.2022.104784.

[2] IAEA-EBP-WWER-08 (2006). Guidelines on Pressurised Thermal Shock Analysis for WWER Nuclear Power Plants, IAEA-EBP-WWER-08, Rev. 1, International Atomic Energy Agency, Vienna.

[3] IAEA-TECDOC-1627 (2010). Pressurized Thermal Shock in Nuclear Power Plants: Good Practices for Assessment, IAEA-TECDOC-1627, International Atomic Energy Agency, Vienna.

[4] Brumovsky M. and Martin O., (2024). VERLIFE Guidelines for integrity and lifetime assessment of components and piping in WWER nuclear power plants, Publ. Off. of the Eur. Un., Luxembourg, pp. 256. DOI: https://dx.doi.org/10.2760/529703.

[5] Fekete, T. (2016). Review of pressurized thermal shock studies of large scale reactor pressure vessels in Hungary. Fracture and Structural Integrity, 10(36), Pages 99–111. DOI: https://doi.org/10.3221/IGF-ESIS.36.10.

[6] Chou, H.-W., Shen, Y.-Y. and Huang, C.-C. (2019). Development of pressure–temperature operation limits for a PWR vessel considering beltline shell and extended beltline nozzles, Int. J. Press. Vessels Pip. DOI: https://doi.org/10.1016/j.ijpvp.2019.103944.
[7] API, ASME, (2016). API 579-1/ASME FFS-1: Fitness-For-Service, American Petroleum Institute; American Society of Mechanical Engineers.
[8] ASME, (2023). ASME Boiler and Pressure Vessel Code, Section XI: Rules for Inservice Inspection of Nuclear Power Plant Components, American Society of Mechanical Engineers.
[9] Li, Y., Jin, T., Wang, Z. and Wang, D. (2020). Engineering critical assessment of reactor pressure vessels with nozzle corner cracks under pressurized thermal shocks, Nucl. Eng. Technol. DOI: https://doi.org/10.1016/j.net.2020.04.019.
[10] Lee, C.-H. and Chou, H.-W. (2022). Stress intensity factor assessment for reactor pressure vessel nozzles containing postulated corner cracks, Eng. Fract. Mech. DOI: https://doi.org/10.1016/j.engfracmech.2022.108838.
[11] Chapuliot, S. (2016). Stress intensity factor calculation in sharp and beveled edge nozzle corners, Int. J. Press. Vessels Pip. DOI: https://doi.org/10.1016/j.ijpvp.2016.03.015.
[12] Wang D., Jin T., Duan Y., Li Y., Liu, Liu Y., Xu X. (2025) Stress intensity factor solution for pressurized vessel nozzle corner crack subjected to an arbitrary stress distribution using the influence coefficient method, Int. J. Press. Vessels Pip. DOI: https://doi.org/10.1016/j.ijpvp.2025.105519.
[13] Lu K., Li X., Wu Z., Wang D., Pan J., Zhang T. (2025) Numerical investigation on stress intensity factor solutions of nozzle corner cracks in reactor pressure vessels, Int. J. Press. Vessels Pip. DOI: https://doi.org/10.1016/j.ijpvp.2025.105584.
[14] Keeney, J.A. and Bryson, J.W. (1995). Stress-intensity-factor influence coefficients for semi-elliptical inner-surface flaws in clad pressure vessels, Fracture Mechanics, 26, pp. 430–443.
[15] Liu, C., Jiao, G. C., Chandwani, R., & Timbrell, C. (2021). Study on application range of SIF calculation method for nozzle corner crack in pressure vessel for ASME XI code. International Journal of Pressure Vessels and Piping, 193. DOI: https://doi.org/10.1016/j.ijpvp.2021.104478.
[16] Marie, S. and Chapuliot, S. (2008). Improvement of the calculation of the stress intensity factors for underclad and through-clad defects in a reactor pressure vessel subjected to a pressurised thermal shock, Int. J. Press. Vessels Pip., pp. 517–531. DOI: https://doi.org/10.1016/j.ijpvp.2008.02.006.